https://doi.org/10.1016/j.enconman.2018.10.027

Manuscript prepared for Energy Conversion and Management

Soil thermal imbalance of ground source heat pump systems with spiral-coil energy pile groups under seepage conditions and various influential factors

Tian You[a,*], Xianting Li[b], Sunliang Cao[a], Hongxing Yang[a,*]

a Renewable Energy Research Group, Department of Building Services Engineering, The Hong Kong Polytechnic University, Hong Kong, China

b Department of Building Science, Beijing Key Lab of Indoor Air Quality Evaluation and Control, School of Architecture, Tsinghua University, Beijing, China

* Corresponding author: Dr Tian You

Renewable Energy Research Group, Department of Building Services Engineering, The Hong Kong Polytechnic University, Hong Kong, China

Tel.: +852-5425-1572

Fax: +852-2765-7198

E-mail: tian.you@polyu.edu.hk

* Corresponding author: Prof. Hongxing Yang

Renewable Energy Research Group, Department of Building Services Engineering, The Hong Kong Polytechnic University, Hong Kong, China

Tel.: +852-2766-5863

Fax: +852-2765-7198

E-mail: hong-xing.yang@polyu.edu.hk

Abstract

Soil thermal imbalance of heating-dominant ground source heat pump systems with a large number of energy piles without appropriately designed configurations will be more likely to cause the soil temperature decrease and the heating performance degradation for long-term operation. The ground source heat pump systems with spiral-coil energy piles are promising for building energy saving in high-density cities. To analyze the effect of different influential factors on the soil thermal imbalance of these systems, an analytical model for spiral-coil energy pile group under seepage conditions is proposed, considering different heat fluxes of different piles and time variation of heat fluxes. A sandbox experiment is set up to validate the precision of the proposed model. Based on the proposed model, the ground source heat pump system model is further established to investigate the system performance. Results show that 1) the energy piles in the outer layers of group, at the upstream of seepage flow direction, with large pile spacing, or arranged in a line shape can exchange more heat with soil; 2) the groundwater effectively alleviates the temperature decreases of soil near the energy piles and located at the upstream; 3) the groundwater flow, slim pile layout, large pile spacing, and short pile length are effective to alleviate the decreases of outlet fluid temperature and heating coefficient of performance, contributing to higher heating capacity and lower energy consumption.

Keywords: soil thermal imbalance; energy pile; spiral coil; analytical model; groundwater; ground source heat pump

Nomenclature

a	thermal diffusion coefficient, m^2/s
b	coil pitch, m
c	specific heat, J/(kg·K)
G	volumetric flow rate, m^3/s
H	depths of the pile, m
h	convective heat transfer coefficient of the fluid, $W/(m^2 \cdot K)$
L	length, m
m	mass flow rate, kg/s
P	power consumption of the heat pump unit, kW
Q	heat capacity of the heat pump unit, kW
q	heat flux, W/m
R	thermal resistance, (°C·m)/W
r	radius, m
t	temperature, °C
u	velocity of groundwater flow, m/s
x, y, z	coordination of points in the soil, m

Greek letters

Θ	dimensionless excess temperature
τ	time, s
θ	excess soil temperature, °C
λ	the thermal conductivity, W/(m·K)
η	efficiency of the water pump

Abbreviations

DeST	Designer's Simulation Toolkit
GHX	ground heat exchanger
GSHP	ground source heat pump
SEPGS	the analytical model for spiral-coil energy pile group with seepage
SSEPS	the model of single spiral-coil energy pile with seepage

Subscript

b	spiral pipe wall
c	cooling mode
ci	condenser inlet

co	condenser outlet
ei	evaporator inlet
f	Fluid
h	heating mode
hp	heat pump unit
in	inlet fluid of the spiral pipe
ni	serial number of energy piles in the soil (*ni*=1, 2, …, *N*)
out	outlet fluid of the spiral pipe
s	Soil
wp	water pump

1 Introduction

Ground source heat pump (GSHP) systems use the soil as the heat sink or heat source to provide space heating or cooling for the buildings, reducing the energy consumptions and pollutant emissions [1-3]. These advantages have attracted wide financial incentives from governments [4], stimulating fast-increasing applications all over the world. However, the conventional GSHPs require large land areas for the installation of boreholes, which prevents the wider applications in dense cities. GSHPs with energy piles [5-7], of which the ground heat exchangers are buried inside the building pile foundations, can greatly reduce the land occupation and drilling cost, attracting increasing attention from researchers and engineers [8-9]. Amongst different pipes inside the energy piles, the spiral pipes attached to the reinforcement cage perform well in heat transfer [10-12]. However, problems caused by soil thermal imbalance remain to be solved in heating-dominant GSHP systems [13-14]. Since the accumulated heating load is far higher than the accumulated cooling load (on an annual basis) in these systems, the heat extracted from the soil is much more than that injected into it. This cold accumulation in the soil will cause the soil temperature decrease [15] and the heating performance decline year after year. In addition, the imbalance is aggravated in energy pile groups due to less heat dissipation boundaries per soil volume, leading to more serious problems. The parameters of spiral-coil energy pile groups, including pile layout, pile spacing, pile depth and groundwater flow, have great influences on the soil heat transfer and the system operating performance. It is of significance to establish accurate heat and mass transfer models of energy pile groups for optimizing the GSHP system design and operation. Currently, the ground heat exchanger (GHX) group models are classified into two types: the analytical models and the numerical models. The current analytical group models mainly target on the U-pipe borehole group, instead of spiral-coil energy pile group with seepage. They assume the same heat flux intensities and same pipe wall temperatures among different boreholes, with the soil temperature directly superposed by the heat contribution of each individual borehole. These models ignore the thermal interaction between boreholes and the heat flux differences among different boreholes located at different positions in a borehole group. Cimmino et al. [16] proposed a borehole group model based on the analytical finite line source model to approximate the g-functions. Li et al. [17], Yu et al. [18] and Rang [19] assumed the same heat fluxes among different boreholes to analyze the soil temperature variation, while the convective heat transfer of fluid inside the pipe was ignored. Katsura et al. [20] reduced the calculation time of analytical models for multiple ground heat exchangers by the approximation of the temperature responses in different time scales. Co et al. [21] proposed the analytical model of a single energy pile and assumed the same heat fluxes for different energy piles to calculate the dimensionless soil temperature in a pile group with different layouts. The existing numerical GHX group models were usually for two-dimensional simulations, ignoring the influence of pipe depth and fluid velocity inside the pipes. Choi et al. [22] used the two-dimensional coupled heat conduction-convection model to analyze the effect of groundwater flow on the performance of borehole GHX arrays. Loveridge and Powrie [23] used a two-dimensional numerical model to deduce the g-function for multiple energy pile GHXs. Gao et al. [24], Lee and Lam [25] built the 3D numerical models of a single energy pile, but these models were not suitable for a group of energy piles due to the heavy calculation load. As a summary, the currently existing models are not suitable to analyze the variable outlet fluid temperature and heat transfer of energy pile groups, as well as the transient performance of GSHP systems with energy piles under seepage conditions and unbalanced building loads. The influences of different factors on the soil thermal imbalance of GSHP systems with spiral-coil energy piles are also difficult to be analyzed by the currently existing models.

In this paper, an analytical model for spiral-coil energy pile group with seepage (SEPGS model) is proposed. It takes into considerations the different heat fluxes of different piles, the heat interaction between different piles, the actual geometry of spiral coils, the convective heat transfer of fluid inside the pipe, the groundwater flow, the heat transfer of soil surface, and the time variation of pipe heat fluxes. The software DeST (Designer's Simulation Toolkit) is used to simulate the hourly building load for the system analysis. The GSHP system model is established by combining the SEPGS model and other main component models. The influences of groundwater velocity, pile layout, pile spacing, and pile depth on the soil thermal imbalance of GSHP system will be investigated. This study aims to facilitate better design of GSHP systems with SEPGS model to alleviate the performance decline caused by soil thermal imbalance.

2 Principles of the SEPGS model

In this section, the SEPGS model is derived from the model of single spiral-coil energy pile with seepage (SSEPS model) by applying the superposition principle through matrix operations. A sandbox experiment is further set up to validate the accuracy of the proposed model for GHX groups.

2.1 Basic theories

2.1.1 The SSEPS model

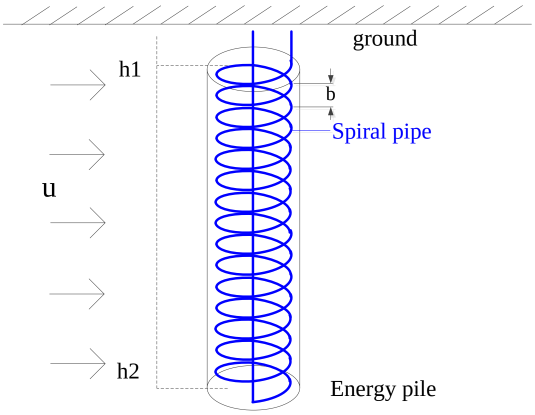

Figure 1 Diagram of a single spiral-coil energy pile with seepage

The diagram of a single coil energy pile with seepage is shown in Figure 1. Zhang [26, 27] proposed an SSEPS model based on the Green function, as shown in Equation (1). The soil is considered as a semi-infinite medium with a homogeneous initial temperature and the soil surface keeps a constant initial temperature. The pipe in energy pile is deemed as a finite spiral coil. The medium outside the spiral pipe is sole soil. Besides, the homogeneous groundwater flow with a constant velocity is considered in the model.

The dimensionless excess soil temperatures influenced by the seepage and the pile geometry at different coordinates and different time are the integral of Green function along the spiral line and over the releasing time of constant heat fluxes. Based on Equation (1), the dimensionless excess soil temperature has no relationship with the value of the heat flux. The dimensionless excess soil temperature at τ^{th} time step (Θ) stands for the excess soil temperature at τ^{th} time step ($\theta = t - t_0$) divided by the constant heat flux of an energy pile starting from the initial time step (q_l) (Equation (1a)).

$$\Theta=\frac{B}{16\pi^{5/2}}\int_0^{Fo}\frac{1}{\left(Fo-Fo'\right)^{3/2}}\int_{2\pi H_1/B}^{2\pi H_2/B}\exp\left[-\frac{\left[X-\cos\varphi'-S\left(Fo-Fo'\right)\right]^2+\left(Y-\sin\varphi'\right)^2}{4\left(Fo-Fo'\right)}\right]\times$$
$$\left\{\exp\left[-\frac{\left(Z-B\varphi'/2\pi\right)^2}{4\left(Fo-Fo'\right)}\right]-\exp\left[-\frac{\left(Z+B\varphi'/2\pi\right)^2}{4\left(Fo-Fo'\right)}\right]\right\}d\varphi'dFo' \tag{1}$$

$$\Theta=\frac{\lambda_s\times\theta}{q_l}=\frac{\lambda_s\times\left(t-t_0\right)}{q_l} \tag{1a}$$

where Θ is the dimensionless excess temperature; the dimensionless parameters are $\mathrm{B}=\frac{b}{r_0}$, $\mathrm{Fo}=\frac{a\tau}{r_0^2}$, $\mathrm{X}=\frac{x}{r_0}$, $\mathrm{Y}=\frac{y}{r_0}$, $\mathrm{Z}=\frac{z}{r_0}$, $\mathrm{H}_1=\frac{h_1}{r_0}$, $\mathrm{H}_2=\frac{h_2}{r_0}$, $\mathrm{S}=\frac{ur_0}{a}$; b is the coil pitch, m; r_0 is the radius of spiral coil, m; a is the thermal diffusion coefficient, m^2/s; τ is the time, s; x, y, z is the coordination of points in the soil, m; h_1 and h_2 are the depths of the top and bottom of the pile, m; u is the velocity of groundwater flow, m/s; λ_s is the thermal conductivity of the soil, W/(m·K); q_l is the heat flux of the energy pile, W/m; t_0 is the initial soil temperature, °C.

2.1.2 Superposition principle

Assuming that the soil thermal properties are not affected by the temperature, the heat transfer in the infinite soil follows the space and time superposition principle [28]. Based on this principle, the multi-pile model [29] and variable heat fluxes model [30] were deduced, respectively.

(1) Multi-pile model

Following the space superposition principle, the soil temperature influenced by different independent heat fluxes is the superposition of soil temperatures influenced by each heat flux. For the soil encompassing multiple piles, the actual excess soil temperature is the sum of excess soil temperatures influenced by all the energy piles, as shown in Equation (2).

$$\theta(j\Delta\tau)=\sum_{ni=1}^{N}\theta_{ni}(j\Delta\tau) \tag{2}$$

where $\theta_{ni}(j\Delta\tau)$ is the excess soil temperature influenced by the ni^{th} energy pile, °C; ni is the serial number of energy piles in the soil (ni=1, 2, …, N).

(2) Variable heat fluxes model

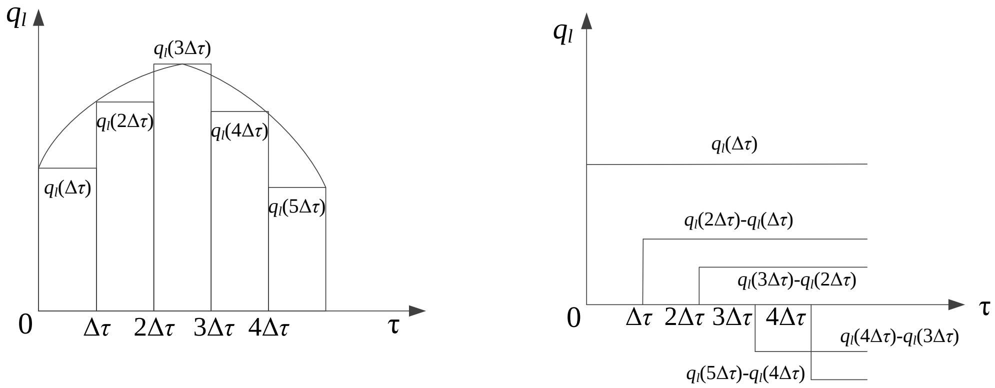

(a) Variable heat fluxes (b) Equivalent constant heat flux differences

Figure 2 Diagram of the superposition of variable heat fluxes

Following the time superposition principle, the soil temperature influenced by variable heat fluxes is the superposition of soil temperatures influenced by each separated constant heat flux difference starting from different time steps. The variable heat fluxes are the sum of all the equivalent constant heat flux differences starting from different time steps, as shown in Figure 2. Therefore, the excess soil temperature under variable heat fluxes is equal to the equivalent constant heat flux differences timing the dimensionless excess soil temperatures at the corresponding time steps, as shown in Equation (3).

$$\theta(j\Delta\tau)=\frac{1}{\lambda_s}\sum_{i=1}^{j}\left[q_l(i\Delta\tau)-q_l((i-1)\Delta\tau)\right]\times\Theta((j-i+1)\Delta\tau) \tag{3}$$

$$q_l(0)=0 \tag{3a}$$

where i, j are the serial numbers of the time step.

2.2 The SEPGS model

The diagram of an energy pile group with variable heat fluxes is illustrated in Figure 3. For the GSHP system, the inlet fluid temperatures of the energy piles in a group are usually identical. Due to different positions in the group, the heat fluxes of different piles are different and the wall temperatures of the spiral pipes are different as well. It should be noted that the wall temperature of each spiral coil is influenced by the heat fluxes of all the energy piles (including the pile itself and all other piles) in the soil. Based on the basic theories of the SSEPS model and the superposition principle, the SEPGS model is proposed in this section.

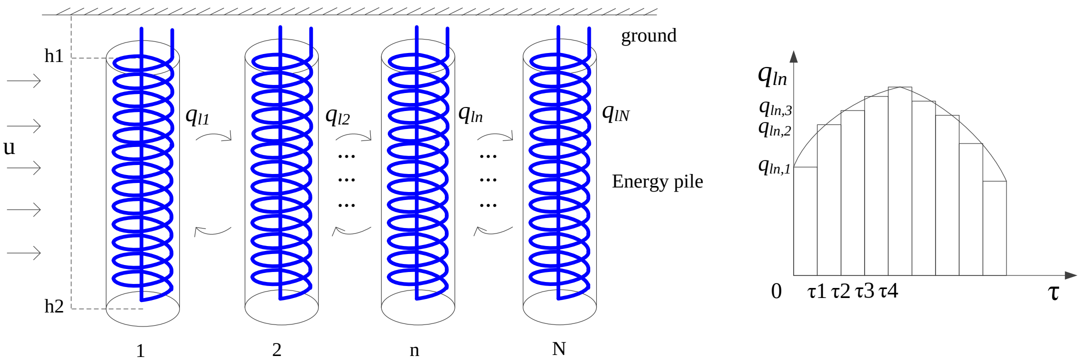

Figure 3 Diagram of energy pile group with variable heat fluxes

2.2.1 Interactions of pipe wall temperatures in the energy pile group

The excess wall temperature of each spiral pipe is influenced by the heat fluxes of all the pipes in the energy pile group all the time. It is calculated by superposing the products of the equivalent constant heat flux differences $[q_{l,ni}(i\Delta\tau)\text{-}\ q_{l,ni}((i\text{-}1)\Delta\tau)]$ and the corresponding dimensionless excess temperatures $[\Theta_{ni,n}((j\text{-}i+1)\Delta\tau)]$ of each energy pile, as shown in Equation (4). In other words, in terms of the heat transfer outside a pipe, the heat flux of an energy pile can be expressed based on the dimensionless excess temperatures and the superposition principle.

$$\theta_{b,n}\left(j\Delta\tau\right)=\frac{1}{\lambda_s}\sum_{ni=1}^{N}\sum_{i=1}^{j}\left[q_{l,ni}\left(i\Delta\tau\right)-q_{l,ni}\left(\left(i-1\right)\Delta\tau\right)\right]\times\Theta_{ni,n}\left(\left(j-i+1\right)\Delta\tau\right) \tag{4}$$

$$\theta_{b,n}\left(j\Delta\tau\right)=t_{b,n}\left(j\Delta\tau\right)-t_0 \tag{4a}$$

where $\theta_{b,n}(j\Delta\tau)$ is the excess wall temperature of the spiral pipe in the n^{th} energy pile at the j^{th} time step, °C; $q_{l,ni}(i\Delta\tau)$ is the heat flux intensity of the ni^{th} energy pile at the i^{th} time step, W/m; $\Theta_{ni,n}((j-i+1)\Delta\tau)$ is the dimensionless excess wall temperature of the spiral pipe in the n^{th} energy pile influenced by the heat flux of the ni^{th} energy pile at the $(j-i+1)^{th}$ time step; $t_{b,n}(j\Delta\tau)$ is the wall temperature of the spiral pipe in the n^{th} energy pile at the j^{th} time step, °C.

To simplify the calculation, the wall temperature at the middle depth (z=0.5H) is used as the average pipe wall temperature of the spiral pipe. Since the dimensionless excess temperatures are influenced by independent different heat sources and have no relationship with the heat fluxes of the heat sources, the dimensionless excess wall temperature of a spiral pipe influenced by the pipe itself and pipes in other energy piles can be calculated in advance based on the SSEPS model.

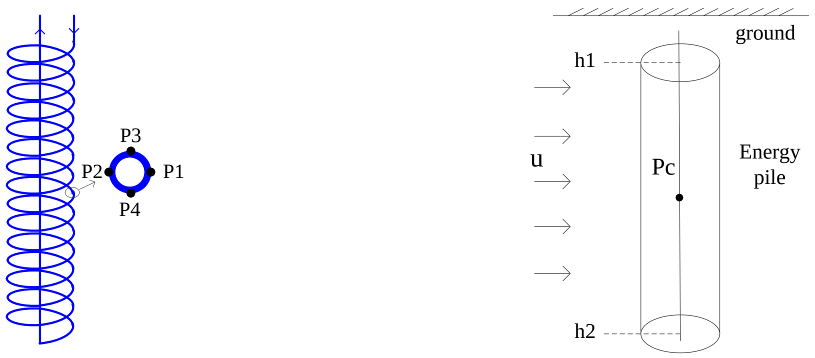

(a) Representative points for the temperature calculation influenced by the pipe itself

(b) Representative points for the temperature calculation influenced by the other energy piles

Figure 4 The representative points of the spiral pipe wall

For the calculation of the dimensionless excess wall temperature influenced by the pipe itself, 4 typical points at the middle depth of the pipe are selected, as shown in Figure 4(a). The dimensionless temperatures of these 4 typical points influenced by the pipe itself are shown in Table 1. For a certain groundwater velocity, the dimensionless temperatures of 4 points are nearly the same with only tiny differences. The average dimensionless temperatures of the 4 points are considered as the dimensionless pipe wall temperatures influenced by the pipe itself. For the calculation of the dimensionless excess wall temperature influenced by the pipes in other energy piles, the center of the cross-section at the middle depth of the energy pile is selected as the typical point, as shown in Figure 4(b). The dimensionless temperatures of this point are considered as the dimensionless pipe wall temperature influenced by pipes in other energy piles. So, Equation (5) can be further deduced from Equation (4).

$$\begin{aligned}&\theta_{b,n}\left(j\Delta\tau\right)\\&=\frac{1}{\lambda_s}\sum_{i=1}^{j}\left[q_{l,n}\left(i\Delta\tau\right)-q_{l,n}\left(\left(i-1\right)\Delta\tau\right)\right]\times\frac{1}{4}\sum_{\mathrm{P_i}=\mathrm{P_1}}^{P_4}\Theta_{n,P_i}\left(\left(j-i+1\right)\Delta\tau\right)\\&+\frac{1}{\lambda_s}\sum_{ni=1(ni\neq n)}^{N}\sum_{i=1}^{j}\left[q_{l,ni}\left(i\Delta\tau\right)-q_{l,ni}\left(\left(i-1\right)\Delta\tau\right)\right]\times\Theta_{ni,P_c}\left(\left(j-i+1\right)\Delta\tau\right)\end{aligned}\quad(5)$$

where $\Theta_{\mathrm{n,P_i}}((j\text{-}i+1)\Delta\tau)$ is the dimensionless excess temperature of $\mathrm{P_i}$ ($\mathrm{P_i}=\mathrm{P_1}\sim\mathrm{P_4}$) in the n^{th} energy pile influenced by the heat flux of the n^{th} energy pile itself at the $(j\text{-}i+1)^{\mathrm{th}}$ time step; $\Theta_{\mathrm{ni,P_c}}((j\text{-}i+1)\Delta\tau)$ is the dimensionless excess temperature of $\mathrm{P_c}$ in the n^{th} energy pile influenced by the heat flux of the ni^{th} energy pile ($ni\neq n$) at the $(j\text{-}i+1)^{\mathrm{th}}$ time step.

Table 1 Dimensionless temperatures of 4 typical points at the middle depth of a spiral pipe

Groundwater velocity	P1	P2	P3	P4
0	0.42452	0.42688	0.42579	0.42565
6×10^{-7} m/s	0.22997	0.22993	0.23004	0.22990

2.2.2 Heat flux matrix of the energy pile group

In terms of the heat transfer inside a pipe, the heat flux of an energy pile is equal to the internal energy variation corresponding to the fluid temperature difference between the inlet and outlet of the whole pipe, as shown in Equation (6).

$$t_{out,n}(j\Delta\tau)=t_{in}(j\Delta\tau)-\frac{q_{l,n}\left(j\Delta\tau\right)\times H}{c_f m_f} \tag{6}$$

where $t_{\mathrm{in}}(j\Delta\tau)$ is the inlet fluid temperature of the spiral pipe at the j^{th} time step, °C; $t_{\mathrm{out,n}}(j\Delta\tau)$ is the outlet fluid temperature of the spiral pipe in the n^{th} energy pile at the j^{th} time step, °C; H is the depth of the energy pile, m; c_{f} is the specific heat of fluid inside the spiral pipe, J/(kg·K); m_{f} is the mass flow rate of fluid, kg/s.

In terms of the heat transfer between the fluid inside and the outer wall of the spiral pipe, the heat flux of the energy pile can be calculated by the method of thermal resistance, as shown in Equation (7). The fluid temperature is approximately equal to the average value between the inlet and outlet fluid temperatures (Equation (7(a))). The thermal resistance between the fluid and the outer wall of the pipe is composed of the thermal conduction resistance ($\frac{1}{2\pi\lambda_p}\ln\frac{r_o}{r_i}$) and thermal convection resistance ($\frac{1}{2\pi r_i h}$) (Equation (7(b))). The convective heat transfer coefficient of the fluid is based on the Nu number and the empirical equations [29] shown in Equation (7(c)) and Equation (7(d)).

$$q_{l,n}\left(j\Delta\tau\right)=\frac{t_{f,n}(j\Delta\tau)-t_{b,n}(j\Delta\tau)}{R_p}\times\frac{L_{pipe}}{H} \tag{7}$$

$$t_{f,n}(j\Delta\tau)=\frac{t_{in}(j\Delta\tau)+t_{out,n}(j\Delta\tau)}{2} \tag{7a}$$

$$R_p = \frac{1}{2\pi\lambda_p}\ln\frac{r_o}{r_i} + \frac{1}{2\pi r_i h} \tag{7b}$$

$$h = \frac{\lambda_f \times Nu}{2r_i} \tag{7c}$$

$$\begin{cases} Nu = 0.023\cdot \mathrm{Re}^{0.8}\cdot \mathrm{Pr}^{0.3} & \mathrm{Re} > 10000 \\ Nu = 0.116\cdot\left(\mathrm{Re}^{2/3} - 125\right)\cdot \mathrm{Pr}^{1/3}\cdot\left[1+\left(\dfrac{2r_i}{L_{pipe}}\right)^{2/3}\right] & 2200 < \mathrm{Re} < 10000 \\ Nu = 1.86\cdot\left(\mathrm{Re}\cdot \mathrm{Pr}\cdot\dfrac{2r_i}{L_{pipe}}\right)^{1/3} & \mathrm{Re} < 2200, \mathrm{Pr} > 0.6 \end{cases} \tag{7d}$$

where L_{pipe} is the length of the spiral pipe in the n$^{\mathrm{th}}$ energy pile, m; R_{p} is the thermal resistance between the fluid and the outer wall of the pipe, (°C·m)/W; $t_{\mathrm{f,n}}(j\Delta\tau)$ is the average fluid temperature of the spiral pipe in the n$^{\mathrm{th}}$ energy pile, °C; $t_{\mathrm{b,n}}(j\Delta\tau)$ is the wall temperature of the spiral pipe in the n^{th} energy pile at the j^{th} time step, °C; λ_{p} is the thermal conductivity of the spiral pipe, W/(m·K); r_{i} and r_{o} are the inner and outer radii of the spiral pipe, m; h is the convective heat transfer coefficient of the fluid, W/(m^2·K); λ_{f} is the thermal conductivity of the fluid, W/(m·K).

Based on Equations (4)~(7), the heat flux of the energy pile can be calculated by 3 different processes, which are the heat transfer outside the spiral pipe, heat transfer inside the spiral pipe, and the heat transfer between the fluid and the outer wall of the spiral pipe. Through the intermediate parameters (the heat flux and pipe wall temperature), the heat transfer outside and inside the spiral pipe can be combined and the heat flux matrix of all the pipes can be constituted to calculate the actual heat flux of each energy pile, as shown in Equation (8). It considers the difference of heat fluxes among different piles and at different time steps. It also considers the heat transfer inside the pipe and the fluid temperature variations.

$$Q_l = A^{-1} \times B \tag{8}$$

$$Q_l = \left[q_{l,1}\left(j\Delta\tau\right) \quad q_{l,2}\left(j\Delta\tau\right) \quad \dots \quad q_{l,n}\left(j\Delta\tau\right) \quad \dots \quad q_{l,N}\left(j\Delta\tau\right) \right]^T \tag{8a}$$

$$A = \begin{bmatrix} \frac{R_p \times H}{L_{pipe}} + \frac{H}{2c_f m_f} + \frac{\Theta_{1,1}(\Delta\tau)}{\lambda_s} & \frac{\Theta_{2,1}(\Delta\tau)}{\lambda_s} & \dots & \frac{\Theta_{n,1}(\Delta\tau)}{\lambda_s} & \dots & \frac{\Theta_{N,1}(\Delta\tau)}{\lambda_s} \\ \frac{\Theta_{1,2}(\Delta\tau)}{\lambda_s} & \frac{R_p \times H}{L_{pipe}} + \frac{H}{2c_f m_f} + \frac{\Theta_{2,2}(\Delta\tau)}{\lambda_s} & \dots & \frac{\Theta_{n,2}(\Delta\tau)}{\lambda_s} & \dots & \frac{\Theta_{N,2}(\Delta\tau)}{\lambda_s} \\ \dots & \dots & & \dots & & \dots \\ \frac{\Theta_{1,n}(\Delta\tau)}{\lambda_s} & \frac{\Theta_{2,n}(\Delta\tau)}{\lambda_s} & \dots & \frac{R_p \times H}{L_{pipe}} + \frac{H}{2c_f m_f} + \frac{\Theta_{n,n}(\Delta\tau)}{\lambda_s} & \dots & \frac{\Theta_{N,n}(\Delta\tau)}{\lambda_s} \\ \dots & \dots & & \dots & & \dots \\ \frac{\Theta_{1,N}(\Delta\tau)}{\lambda_s} & \frac{\Theta_{2,N}(\Delta\tau)}{\lambda_s} & \dots & \frac{\Theta_{n,N}(\Delta\tau)}{\lambda_s} & \dots & \frac{R_p \times H}{L_{pipe}} + \frac{H}{2c_f m_f} + \frac{\Theta_{N,N}(\Delta\tau)}{\lambda_s} \end{bmatrix} \tag{8b}$$

$$B = \begin{bmatrix} t_{in}\left(j\Delta\tau\right) - t_0 + \sum_{ni=1}^{N} \left\{ q_{l,ni}\left(\left(j-1\right)\Delta\tau\right) \times \Theta_{ni,1}\left(\Delta\tau\right) - \sum_{i=2}^{j-1} \left[q_{l,ni}\left(i\Delta\tau\right) - q_{l,ni}\left(\left(i-1\right)\Delta\tau\right) \right] \times \Theta_{ni,1}\left(\left(j-i+1\right)\Delta\tau\right) - q_{l,ni}\left(\Delta\tau\right) \times \Theta_{ni,1}\left(j\Delta\tau\right) \right\} \Big/ \lambda_s \\ t_{in}\left(j\Delta\tau\right) - t_0 + \sum_{ni=1}^{N} \left\{ q_{l,ni}\left(\left(j-1\right)\Delta\tau\right) \times \Theta_{ni,2}\left(\Delta\tau\right) - \sum_{i=2}^{j-1} \left[q_{l,ni}\left(i\Delta\tau\right) - q_{l,ni}\left(\left(i-1\right)\Delta\tau\right) \right] \times \Theta_{ni,2}\left(\left(j-i+1\right)\Delta\tau\right) - q_{l,ni}\left(\Delta\tau\right) \times \Theta_{ni,2}\left(j\Delta\tau\right) \right\} \Big/ \lambda_s \\ \dots \\ t_{in}\left(j\Delta\tau\right) - t_0 + \sum_{ni=1}^{N} \left\{ q_{l,ni}\left(\left(j-1\right)\Delta\tau\right) \times \Theta_{ni,n}\left(\Delta\tau\right) - \sum_{i=2}^{j-1} \left[q_{l,ni}\left(i\Delta\tau\right) - q_{l,ni}\left(\left(i-1\right)\Delta\tau\right) \right] \times \Theta_{ni,n}\left(\left(j-i+1\right)\Delta\tau\right) - q_{l,ni}\left(\Delta\tau\right) \times \Theta_{ni,n}\left(j\Delta\tau\right) \right\} \Big/ \lambda_s \\ \dots \\ t_{in}\left(j\Delta\tau\right) - t_0 + \sum_{ni=1}^{N} \left\{ q_{l,ni}\left(\left(j-1\right)\Delta\tau\right) \times \Theta_{ni,N}\left(\Delta\tau\right) - \sum_{i=2}^{j-1} \left[q_{l,ni}\left(i\Delta\tau\right) - q_{l,ni}\left(\left(i-1\right)\Delta\tau\right) \right] \times \Theta_{ni,N}\left(\left(j-i+1\right)\Delta\tau\right) - q_{l,ni}\left(\Delta\tau\right) \times \Theta_{ni,N}\left(j\Delta\tau\right) \right\} \Big/ \lambda_s \end{bmatrix} \tag{8c}$$

where Q_l is the matrix of heat fluxes of different energy piles.

2.2.3 Soil temperature distribution

After the calculation of variable heat fluxes of all the pipes, the soil temperature distributions can be achieved based on Equation (9). It is the superposition of the products of equivalent constant heat flux differences $[q_{l,ni}(i\Delta\tau)- q_{l,ni}((i-1)\Delta\tau)]$ and the corresponding dimensionless excess soil temperatures $[\Theta_{ni,s}((j-i+1)\Delta\tau)]$ of each energy pile.

$$\theta_s\left(j\Delta\tau\right) = \frac{1}{\lambda_s} \sum_{ni=1}^{N} \sum_{i=1}^{j} \left[q_{l,ni}\left(i\Delta\tau\right) - q_{l,ni}\left(\left(i-1\right)\Delta\tau\right) \right] \times \Theta_{ni,s}\left(\left(j-i+1\right)\Delta\tau\right) \tag{9}$$

where the subscript *s* denotes the point in the soil for temperature calculation.

2.3 Model validation

Since the SSEPS model had already been validated in the previous research [26], the proposed SEPGS model can be validated as long as the calculation method for GHX group is validated. In this part, the calculation method of GHX group is validated by a sandbox experiment. The experiment rig set up is composed of a sandbox, five U pipes, a water bath, thermocouples, a glass rotameter and a data logger. The 1m ×1m ×1m sandbox is filled with sand, and the homogeneous initial temperature is 21 °C. Five U pipes are buried in the sand with the layout shown in Figure 5. The inlet temperatures of all the pipes are kept constant at 31 °C by a water bath. The water pump with a constant frequency is used for the water circulation. A glass rotameter with testing uncertainty about ±0.1 LPM monitors the total flow rate of five pipes. The flow rate is measured to be constant at about 4 L/min. Four T-type thermocouples are placed next to the central pipe at the depth of 0.5 m to test the sand temperature variations, as shown in Figure 5(b). The testing range of the thermocouples is -10~40 °C and the testing uncertainty is ±0.5 °C. The thermophysical properties of sand are tested by the cutting-ring method, drying method, and the transient hot-wire method [31-33]. The results show that the density and thermal diffusivity of sand are respectively 1.26 g/cm^3 and 0.24 mm^2/s.

(a) The sandbox (b) The layout of U pipes

Figure 5 The sandbox experiment rig

The sand temperature variations of four typical points are measured by the thermocouples for 24 hours. They are also simulated by the analytical calculation method of GHX group based on Equations (8) ~ (9). The result comparisons of both experiment and analytical GHX group model are illustrated in Figure 6. For a certain soil point, the temperature variations obtained by both methods have the same trend and the absolute errors are less than 0.25 °C. Consequently, the analytical model for GHX group can be validated well by the experiment. The accuracy of the proposed SEPGS model can be validated as well.

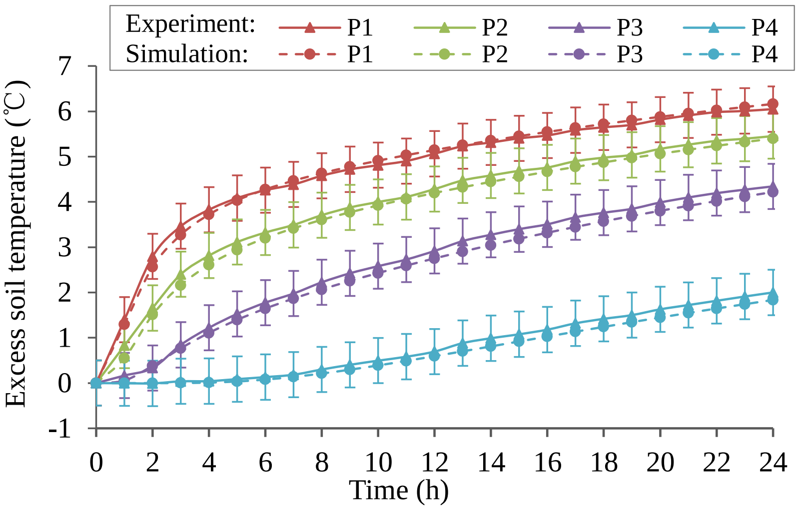

Figure 6 The soil temperature variation obtained by experiment and simulation

3 System model and design

In this section, the GSHP system model is built based on the SEPGS model and other main component models for long-term simulations.

3.1 Building model

A 6200 m^2 residential building in Beijing is selected for simulation. The heating season is 15^{th} November ~ 15^{th} March and the cooling season is 1^{st} June ~ 31^{th} August. The hourly building load is simulated using DeST and the result is shown in Figure 7(a). A time step of one month is selected for the system simulation, so the monthly building load is derived from the hourly load. The maximum monthly heating and cooling loads are respectively 27.24 W/m^2 and -8.35 W/m^2. The accumulated heating load is about 60.93 MWh in a whole heating season, which is much higher than the accumulated cooling load (13.89 MWh) in a cooling season.

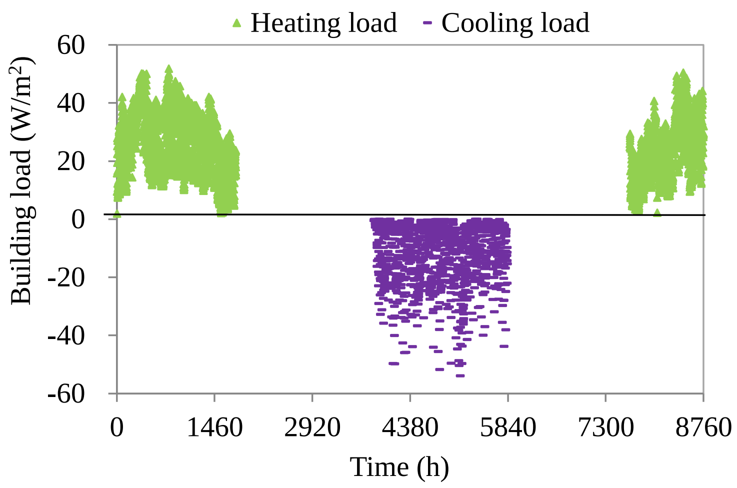

(a) Hourly building load

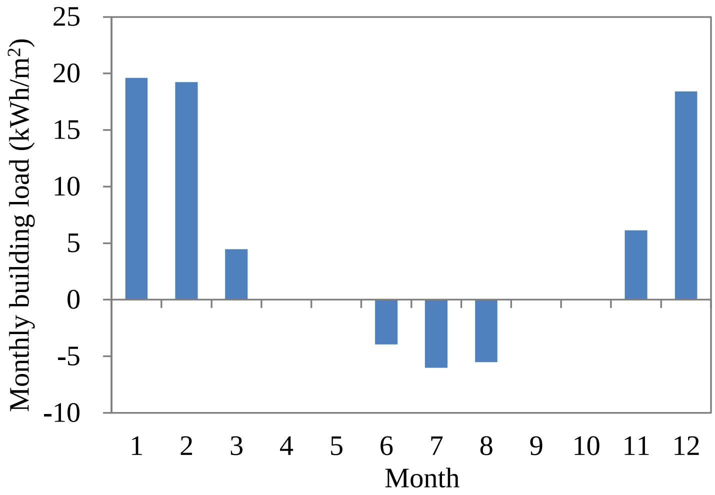

(b) Monthly building load

Figure 7 Heating and cooling loads of the residential building

3.2 Heat pump model

The heat pump model is fitted based on the manufacturer performance catalog [34], as shown in Equation (10). The capacity and power consumption of the heat pump for heating and cooling are determined by the fluid temperatures of the evaporator and condenser.

$$Q_{hp,h} = 5.91t_{ei} - 1.24t_{co} + 162.99 \quad (10a)$$

$$P_{hp,h} = 0.46t_{ei} + 0.64t_{co} + 5.78 \quad (10b)$$

$$Q_{hp,c} = -1.64t_{ci} + 201.21 \quad (10c)$$

$$P_{hp,c} = 0.65t_{ci} + 22.40 \quad (10d)$$

where Q is the heat capacity of the heat pump unit, kW; P is the power consumption of the heat pump unit, kW; t is the fluid temperature, ºC; the subscript hp stands for the heat pump unit; h and c stand for heating and cooling mode, respectively; ei, ci, and co stand for the fluid temperatures at the evaporator inlet, condenser inlet, and condenser outlet, respectively.

3.3 Water pump model

The water pump model is shown in Equation (11). The flow rate of the water pump (G_{wp}) is determined by the water temperature difference and the heat capacity of the heat exchanger in the circuit. The water head of the pump (H_{wp}) is determined by the flow resistance. Based on the flow rate and the water head, the power of the water pump (P_{wp}) can be calculated.

$$P_{wp} = \frac{G_{wp} \times H_{wp}}{\eta} \tag{11}$$

where G is the volumetric flow rate, m^3/s; H is the water head, kPa; η is the efficiency of the water pump, 0.6; the subscript *wp* stands for the water pump.

3.4 GSHP system design

The schematic diagram of the GSHP system with spiral-coil energy pile group under seepage condition is shown in Figure 8. The main components of the system are the building, heat pump, energy piles and water pumps. Based on the SEPGS model, building model, heat pump model and the water pump model, the GSHP system model can be established.

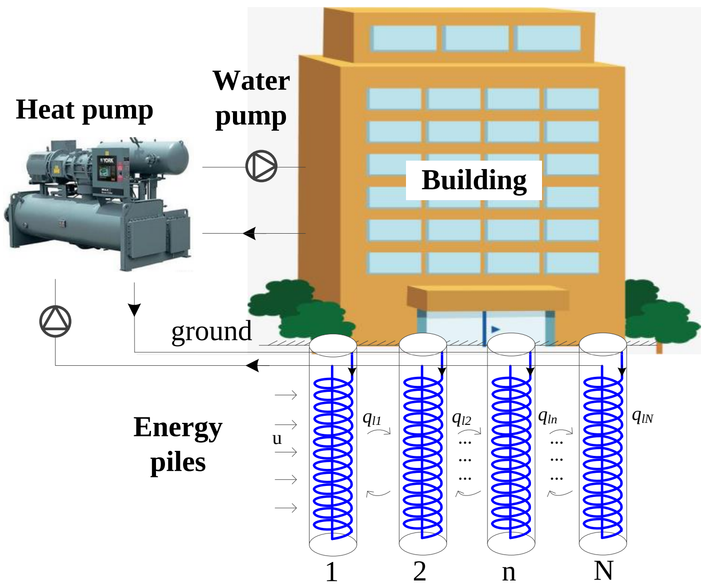

Figure 8 Schematic diagram of the ground source heat pump system with energy piles

To satisfy the heating and cooling demand of the building, the heating capacity of the heat pump is designed as 178.6 kW under the rated condition (the inlet water temperature of the evaporator is 0 ºC and the outlet water temperature of the condenser is 40 ºC). A group of 25 spiral-coil energy piles is designed according to the pre-simulation. The initial soil temperature is 14 ºC in Beijing, which is 1.5 ºC higher than the local average annual air temperature [34]. The thermal conductivity, density and specific heat of soil are respectively 1.74 W/(m·K), 1690 kg/m^3, and 1800 J/(kg·K).

To analyze the influence of different factors, including the groundwater velocity, pile layout, pile spacing as well as the pile depth on the system performance, different cases are simulated. The parameter designs of the energy pile group in different cases are shown in Table 2. The investigated influential factor is changed while other factors are kept the same in a contrasting case group. The velocity of groundwater flow is set to 0, 3×10^{-7} m/s, and 6×10^{-7} m/s. The pile layout includes a matrix shape, a stripe shape, and a line shape, as shown in Figure 9. The pile spacing can be 3 m, 5 m, and 7 m. The pile depth is designed as 10 m, 30 m, and 50 m. For case groups 1 to 3, the energy piles in each case have the same total pipe length and are designed to meet all the building loads in the first year. However, in case group 4, as the energy piles with different pile depths have different total pipe lengths, the total capacities provided by all the energy piles in each case are different while the provided capacities per depth of the energy pile are the same.

Table 2 Parameter designs of the energy pile group

Case groups	Influential factor	Other factors
1	Groundwater velocity: 0, 3×10^{-7} m/s, 6×10^{-7} m/s	Pile layout: matrix shape, Pile spacing: 5 m, Pile depth: 50 m
2	Pile layout: matrix shape, stripe shape, line shape	Groundwater velocity: 0, Pile spacing: 5 m, Pile depth: 50 m
3	Pile spacing: 3 m, 5 m, 7 m	Pile layout: matrix shape, Groundwater velocity: 0, Pile depth: 50 m
4	Pile depth: 10 m, 30 m, 50 m	Pile layout: matrix shape, Groundwater velocity: 0, Pile spacing: 5m,

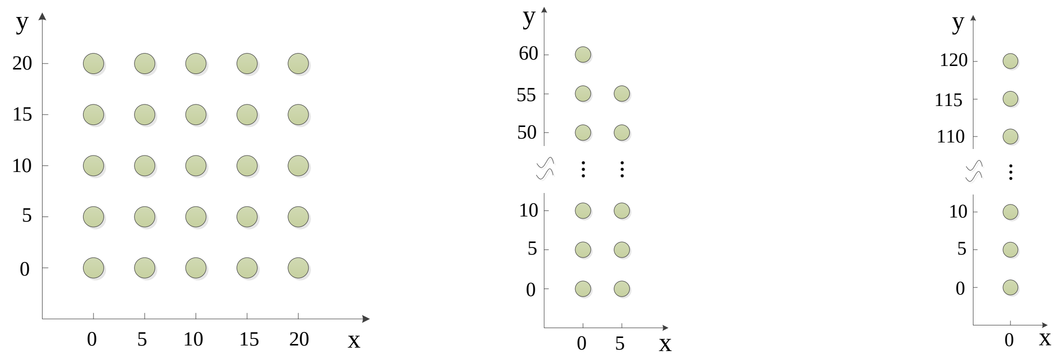

(a) Matrix shape (b) Stripe shape (c) Line shape

Figure 9 The layouts of energy pile groups

4 Results

Based on the system model and the system design, the soil thermal characteristics and system heating performance are investigated under different influential factors. In addition, the heat fluxes of different energy piles and the soil temperature distribution are investigated. The outlet fluid temperatures of different energy pile groups and the heating COP variations in 10 years are analyzed under the influences of different factors. The capacity deficiencies of supplied heat compared to the heating load in ten years are simulated in the time step of one month.

4.1 The heat fluxes of different energy piles

For the GSHP system, the inlet fluid temperatures of the energy piles in a group are usually identical. Due to different positions in the soil, the heat fluxes of different piles are various. Figure 10 shows the different heat fluxes of each energy pile at the end of 10 years under different conditions. It can be seen that 1) the energy piles in the outer layers of the groups, 2) the upstream energy piles along the groundwater flow, 3) the energy piles with large pile spacing, and 4) the energy piles arranged in a line shape can exchange more heat with soil. For the energy pile group in a matrix shape with a pile spacing of 5 m and no groundwater (Figure 10(a)), the maximum heat flux of energy pile is about 74.8 W/m in the outside corner while the minimum value is about 63.8 W/m at the center of the group. For the energy pile group with a groundwater velocity of 6×10^{-7} m/s (Figure 10(b)), the maximum heat flux of energy pile is about 104.2 W/m in the upstream outside corner of the group while the minimum value is about 81.9 W/m at the downstream center. For the energy pile group with a pile spacing of 7 m (Figure 10(c)), the maximum and minimum heat fluxes of energy piles are respectively 82.8 W/m and 67.7 W/m. For the energy pile group in a line shape (Figure 10(d)), the maximum and minimum heat fluxes of energy piles are respectively 93.1 W/m and 84.7 W/m. The total heat fluxes of the pile group in Figure 10(a)~(d) are respectively 1701.1 W/m, 2286.2 W/m, 1853.9 W/m, and 2143.5 W/m. The groundwater flow and the line-shape pile layout are more effective to increase the soil heat exchange intensity.

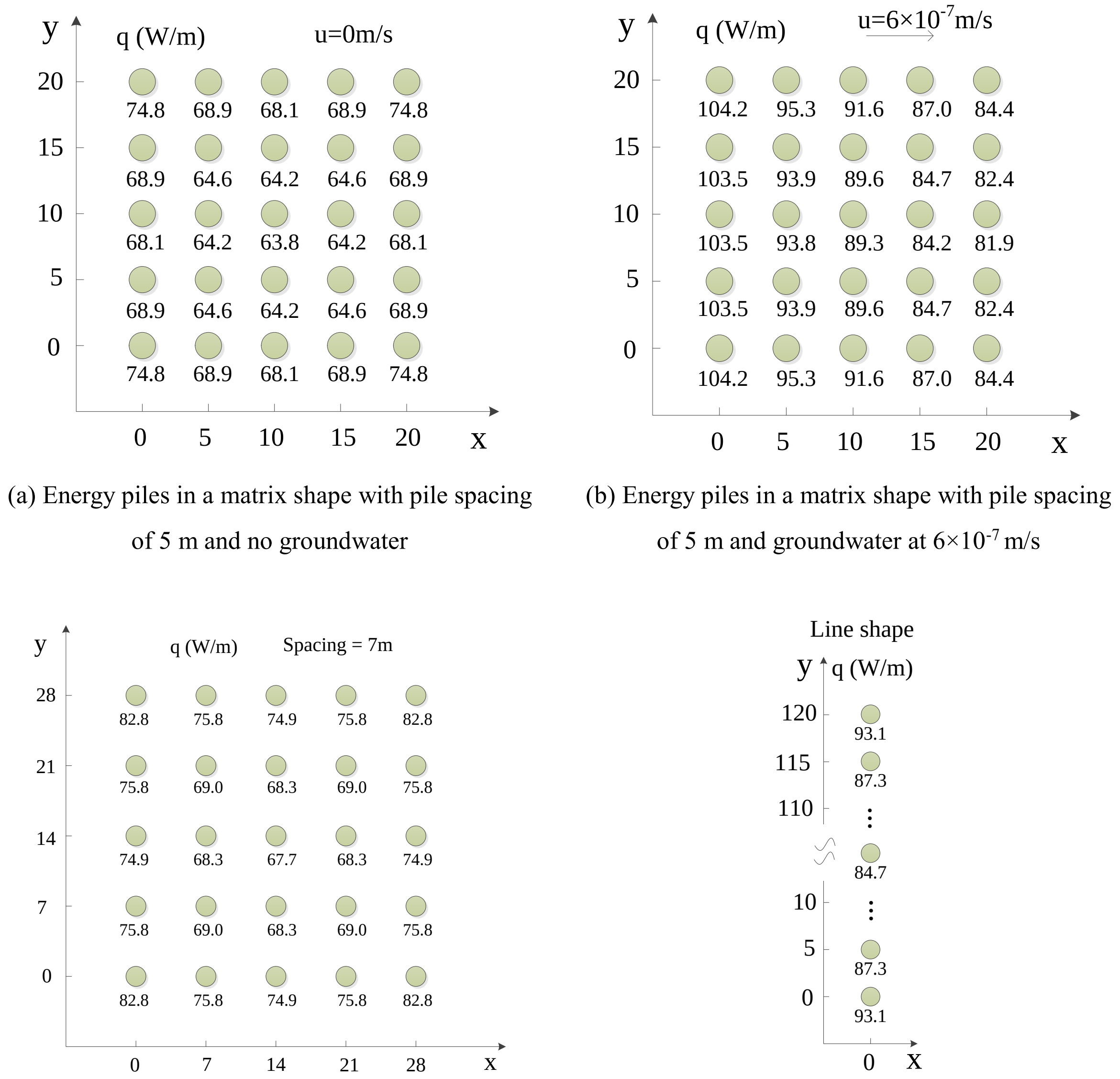

(a) Energy piles in a matrix shape with pile spacing of 5 m and no groundwater

(b) Energy piles in a matrix shape with pile spacing of 5 m and groundwater at 6×10^{-7} m/s

(c) Energy piles in a matrix shape with pile spacing of 7 m and no groundwater

(d) Energy piles in a line shape with pile spacing of 5 m and no groundwater

Figure 10 Heat fluxes of energy piles under different conditions

4.2 The soil temperature distribution after one year

The soil temperature distribution after one operation year (at the end of December) is shown in Figure 11. For the case with no groundwater flow, the soil temperature distribution is symmetrical. The soil temperature near the energy piles is as lowest as 3.2 ºC in the group. For the case with groundwater flow, the soil temperatures in the downstream of groundwater flow can be reduced, while the soil temperatures in the upstream can be increased in the heating season. The groundwater flow can also alleviate the soil temperature decreases near the energy piles. When the velocities of the groundwater flow are 3×10^{-7} m/s and 6×10^{-7} m/s, the lowest soil temperatures in the group are 4.0 ºC and 5.1ºC, respectively.

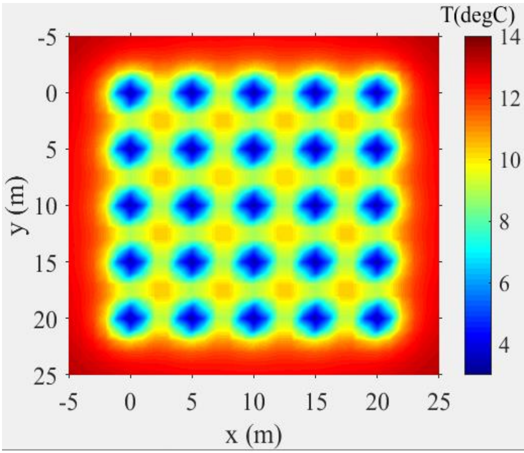

(a) v=0

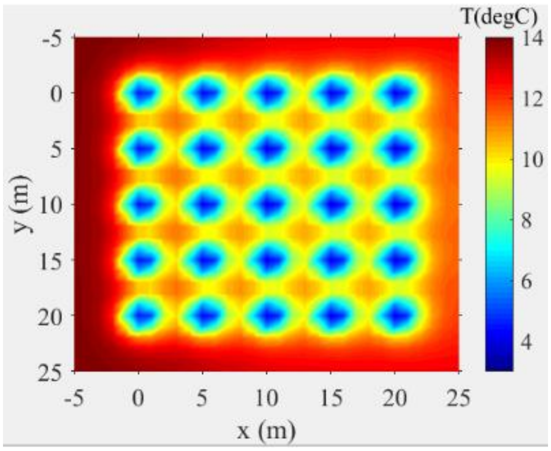

(b) v=3×10^{-7}m/s

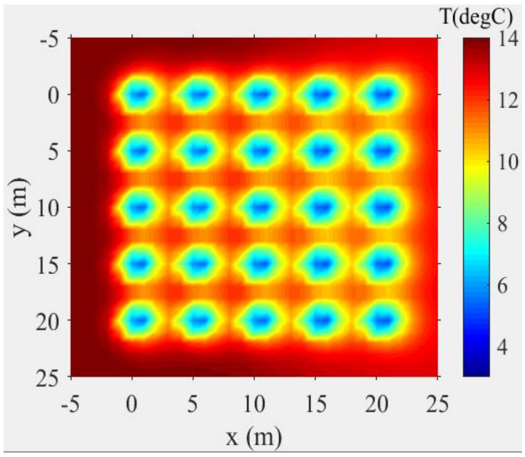

(c) v=6×10^{-7}m/s

Figure 11 Soil temperature distribution influenced by groundwater after one operation year

4.3 Outlet fluid temperature of energy pile group

As mentioned in section 3.1, the heating and cooling loads are unbalanced. It causes a much higher accumulated heat extraction (about 309.5 MWh) than heat injection (about 112.1 MWh) in the first year. Consequently, the soil temperature and outlet fluid temperature decrease year by year. The outlet fluid temperature variations of the energy pile group in 10 years influenced by different factors are illustrated in Figure 12. The groundwater flow, slim pile layout, large pile spacing, and short pile length are effective to alleviate the decrease of outlet fluid temperature.

When the groundwater velocity is 0 m/s, the outlet fluid temperature decreases by 5.4 ºC in the first year. Although the decrease becomes gentle in the following years, the total decrease reaches about 11.8 ºC in 10 years and the minimum outlet fluid temperature is as low as -5.8 ºC. When the seepage exists, the drop in outlet fluid temperature can be effectively mitigated. With groundwater velocities of 3×10^{-7} m/s and 6×10^{-7} m/s, the outlet fluid temperature only decreases by 8.0 ºC and 5.3 ºC in 10 years, respectively.

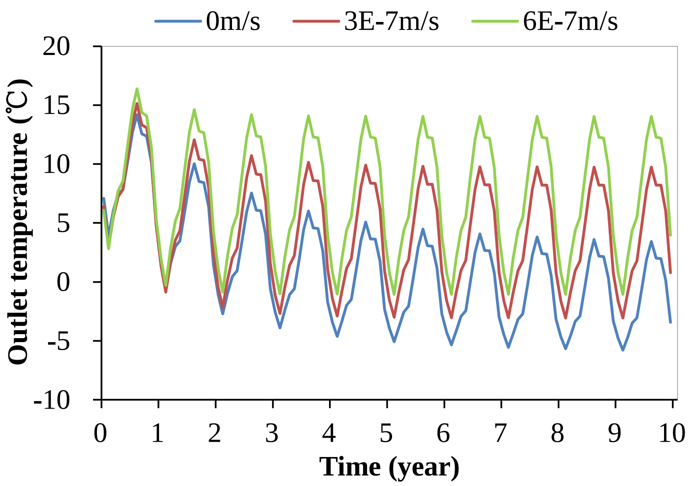

(a) Different groundwater velocities

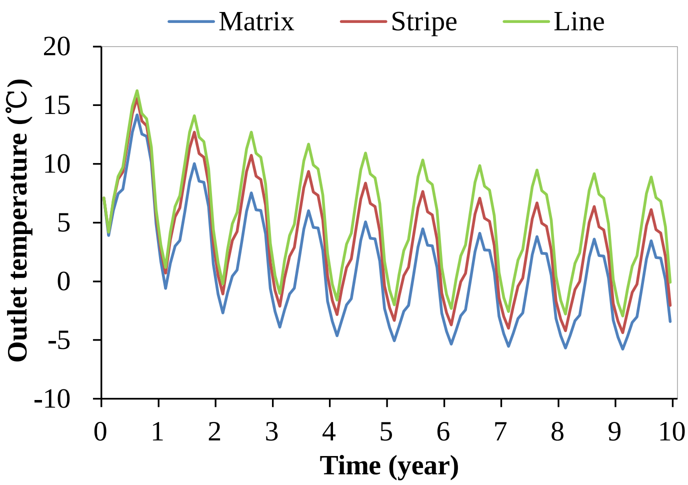

(b) Different pile layouts

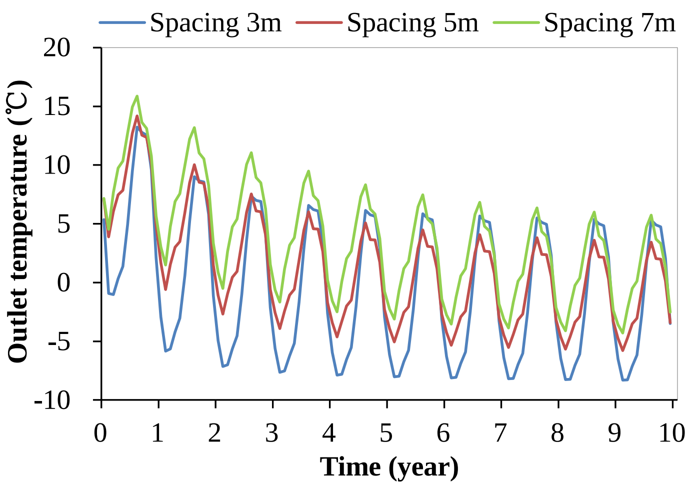

(c) Different pile spacings

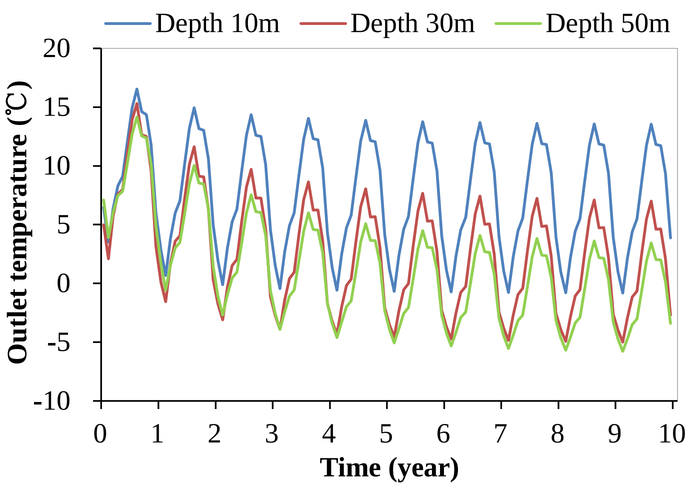

(d) Different pile depths

Figure 12 Outlet fluid temperature of energy pile groups in ten years

When the pile layout is arranged in a stripe shape or line shape (without groundwater flow), the outlet fluid temperature decreases by 10.5 ºC or 9.0 ºC in 10 years. This is because the piles in the slim layout have larger boundary areas per soil volume, which strengthens the heat exchange with the soil outside the energy pile group. In addition, a larger pile spacing can increase the occupied soil volume of a pile group. Consequently, when the pile spacing is 3 m and 7 m, the outlet fluid temperature decreases by 11.9 ºC and 10.7 ºC in 10 years. When the pile depth decreases to 30 m and 10 m, the heat from the soil surface per soil volume becomes higher, which helps the soil temperature recovery and the outlet fluid temperature decreases by 9.0 ºC and 5.5 ºC in 10 years, respectively.

4.4 Heating COP

Since the outlet fluid temperature of the energy pile group decreases year by year caused by the unbalanced building loads, the heating COP of heat pump also declines, as shown in Figure 13. Nonetheless, applying different design modifications can help reduce the deterioration of the heat pump performance.

When the groundwater velocity is 0 m/s, the seasonal average heating COP drops from 3.86 to 2.59 in 10 years. When the groundwater velocity increases to 3×10^{-7} m/s and 6×10^{-7} m/s, the average heating COP in the 10^{th} year increases to 3.11 and 3.46.

When the pile layout is arranged in the stripe shape and line shape, the average heating COP is enhanced to 2.82 and 3.07 in the 10^{th} year. When the pile spacing is changed to 3 m and 7 m, the average heating COP becomes 2.39 and 2.79 in the 10^{th} year. With a decreased pile depth of 30 m and 10 m, average heating COP is improved to 2.75 and 3.47 in the 10^{th} year.

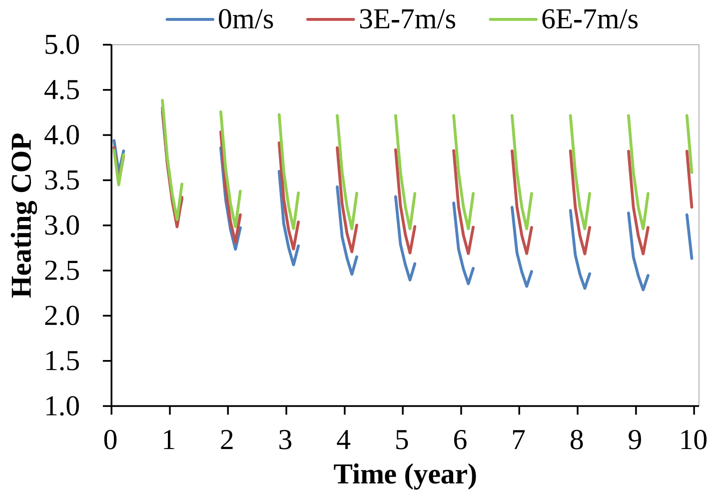

(a) Different groundwater velocities

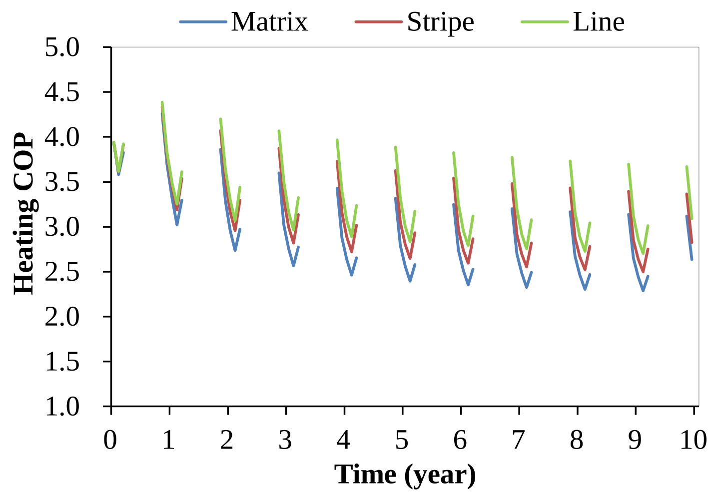

(b) Different pile layouts

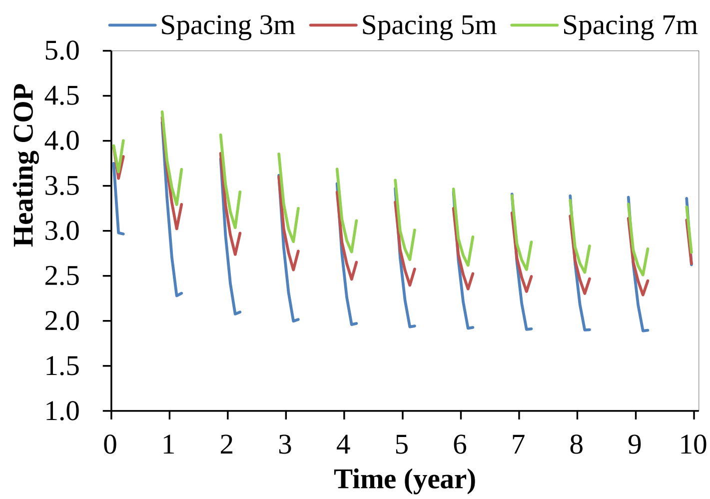

(c) Different pile spacings

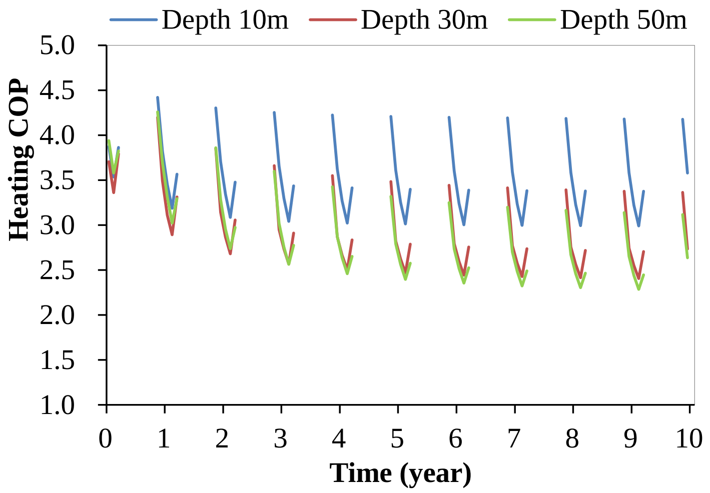

(d) Different pile depths

Figure 13 Heating COP of heat pump unit in ten years

4.5 Heating deficiency

Since the soil imbalance between the heat extraction and injection causes the outlet fluid temperature decrease year by year, the GSHP heating capacity may not meet the building heating load in the following operation years. The heating deficiency is defined as the difference between the supplied heating capacity and required heating load at the same time. The heating deficiencies under different influential factors in 10 years are shown in Figure 14. It indicates that the groundwater flow, slim pile layout, large pile spacing, and short pile length are effective to reduce the heating deficiency.

The heating demands can be satisfied in the first year for all the three different velocities of groundwater flow. However, in the following years, the heating deficiency continuously increases. When the groundwater velocity is 0, the annually accumulated heating deficiency is 83.7 MWh in the 10^{th} year and amounts to 515.7 MWh in total during the ten-year period. When the groundwater velocities are 3×10^{-7} m/s and 6×10^{-7} m/s, the annual heating deficiencies are reduced to 29.0 MWh and 4.7 MWh in the 10th year. The total accumulated heating deficiencies are respectively 211.8 MWh and 35.9 MWh during the ten-year period.

When the piles are arranged in a stripe shape and line shape, the annual heating deficiency is reduced to 56.1 MWh and 29.7 MWh in the 10th year while the total accumulated value is respectively 283.8 MWh and 132.1 MWh in the ten-year period. When the pile spacing is changed to 3 m and 7 m, the annual heating deficiency increases to 112.9 MWh and decreases to 59.9 MWh in the 10th year and the total accumulated value is respectively 894.1 MWh and 286.0 MWh during the ten-year period.

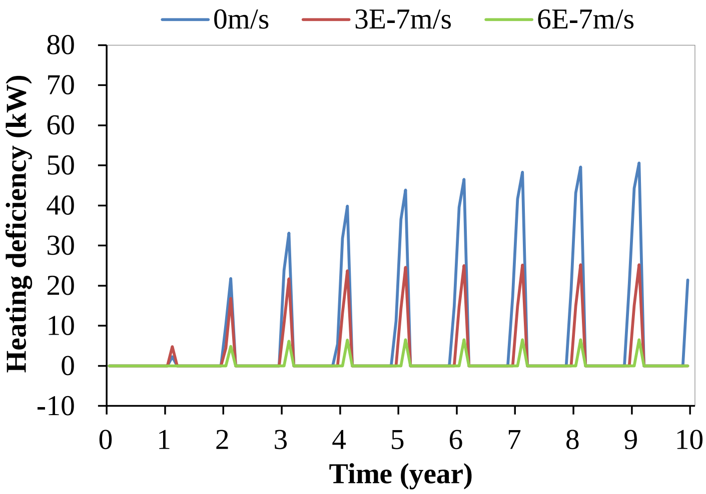

(a) Different groundwater velocities

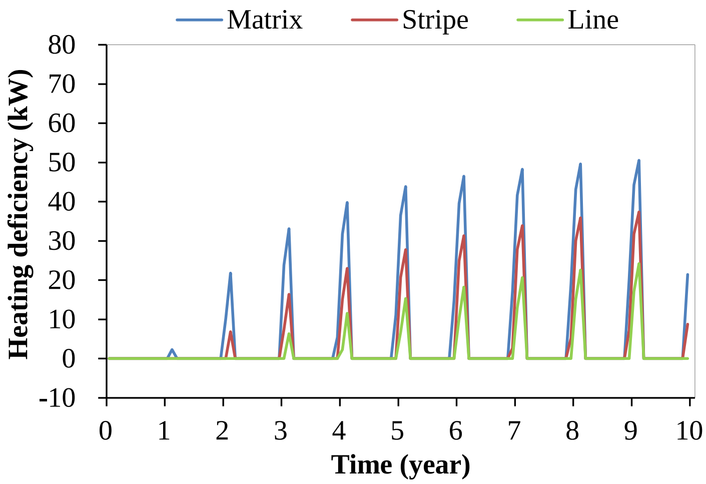

(b) Different pile layouts

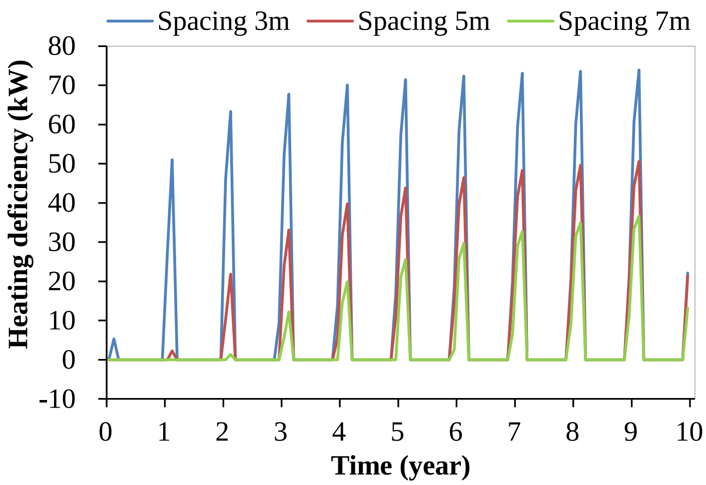

(c) Different pile spacings

Figure 14 Heating deficiency of GSHP system in ten years

Although the heating capacity is deficient under a groundwater velocity of 0 m/s, the decreasing outlet fluid temperature causes declined heating performance, and the total power consumption for heating is still as high as 1312.4 MWh in 10 years. When the groundwater velocity increases to 3×10^{-7} m/s and 6×10^{-7} m/s, the accumulated power consumption for heating decreases to 1286.3 MWh and 1241.4 MWh, respectively.

When the piles are arranged in a stripe shape and line shape, the accumulated power consumption for heating decreases to 1297.9 MWh and 1272.0 MWh, respectively. When the pile spacing is changed to 3 m and 7 m, the accumulated power consumption for heating becomes 1330.0 MWh and 1295.9 MWh, respectively. It can be concluded that the groundwater flow, slim pile layout, and large pile spacing can not only enhance the heating capacity but also lower the power consumption.

5 Conclusion

The analytical SEPGS model is proposed in this paper, considering the influences of the different heat fluxes of piles and the time variation of heat fluxes. The SEPGS model is validated by a sandbox experiment, based on which the GSHP system model is built and the GSHP system with spiral-coil energy piles is designed. The influences of groundwater velocity, pile layout, pile spacing and pile depth on the soil thermal imbalance and long-term performance of the GSHP system are analyzed. The conclusions are drawn as follows:

(1) In the energy pile group, with the same inlet fluid temperature, the heat fluxes of different energy piles are various due to different pile positions in the soil. The energy piles in the outer layers of the groups, the upstream energy piles along the groundwater flow, the energy piles with large pile spacing, and the energy piles arranged in the line shape can exchange more heat with soil.

(2) The comparison of soil temperature distributions shows that the groundwater alleviates the temperature decreases of soil near the energy piles and located upstream. When the groundwater velocity increases from 0 to 3×10^{-7} m/s and 6×10^{-7}m/s, the lowest soil temperature in the group increases from 3.2 ºC to 4.0 ºC and 5.1ºC.

(3) The groundwater flow, slim pile layout, large pile spacing, and short pile length are effective to alleviate the decreases of outlet fluid temperature and system heating COP, contributing to higher heating capacity and lower power consumption.

(4) When the groundwater velocity increases from 0 to 3×10^{-7} m/s and 6×10^{-7} m/s, the outlet fluid temperature drop is respectively reduced from 11.8 ºC to 8.0 ºC and 5.3 ºC in 10 years, the seasonal average heating COP respectively increases from 2.59 to 3.11 and 3.46 in the 10^{th} year, and the heating deficiency respectively decreases from 515.7 MWh to 211.8 MWh and 35.9 MWh in 10 years. When the pile layout is changed from the matrix shape to stripe shape or line shape, the outlet fluid temperature drop is respectively reduced from 11.8 ºC to 10.5 ºC

and 9.0 ºC in 10 years, the seasonal average heating COP respectively increases from 2.59 to 2.82 and 3.07 in the 10th year, and the heating deficiency respectively decreases from 515.7 MWh to 283.8 MWh and 132.1 MWh in 10 years. With the pile spacing increasing from 3 m to 5 m and 7 m, the outlet fluid temperature drop is respectively reduced from 11.9 ºC to 11.8 ºC and 10.7 ºC in 10 years, the seasonal average heating COP respectively increases from 2.39 to 2.59 and 2.79 in the 10th year, and the heating deficiency respectively decreases from 894.1 MWh to 515.7 MWh and 286.0 MWh in 10 years. With the pile depth decreasing from 50 m to 30 m and 10 m, the outlet fluid temperature drop is respectively reduced from 11.8 ºC to 9.0 ºC and 5.5 ºC in 10 years, and the seasonal average heating COP respectively increases from 2.59 to 2.75 and 3.47 in the 10th year.

Acknowledgment

The authors gratefully acknowledge the support of The Hong Kong Polytechnic University's Postdoctoral Fellowships Scheme (1-YW2Y) and the General Research Fund projects of the Hong Kong Research Ground Council (Ref. No.: 152190/14E and 152039/15E).

References

[1] Spitler JD. Editorial: ground-source heat pump system research—past, present, and future. HVAC & R Research, 2005, 11 (2):165–167.

[2] Huang B, Mauerhofer V. Life cycle sustainability assessment of ground source heat pump in Shanghai, China. Journal of Cleaner Production, 2016, 119: 207-214.

[3] Jeong J, Hong T, Kim J, et al. Multi-criteria analysis of a self-consumption strategy for building sectors focused on ground source heat pump systems. Journal of Cleaner

Production, 2018, 186: 68-80.

[4] Majuri P. Ground source heat pumps and environmental policy–The Finnish practitioner's point of view. Journal of Cleaner Production, 2016, 139: 740-749.

[5] Fadejev J, Simson R, Kurnitski J, et al. A review on energy piles design, sizing and modelling. Energy, 2017, 122: 390-407.

[6] Rees S. Advances in ground-source heat pump systems. Woodhead Publishing, 2016.

[7] Park S, Lee D, Lee S, et al. Experimental and numerical analysis on thermal performance of large-diameter cast-in-place energy pile constructed in soft ground. Energy, 2017, 118: 297-311.

[8] Park H, Lee SR, Yoon S, et al. Evaluation of thermal response and performance of PHC energy pile: Field experiments and numerical simulation. Applied Energy, 2013, 103: 12-24.

[9] Hu P, Zha J, Lei F, et al. A composite cylindrical model and its application in analysis of thermal response and performance for energy pile. Energy and Buildings, 2014, 84: 324-332.

[10] Zarrella A, De Carli M, Galgaro A. Thermal performance of two types of energy foundation pile: helical pipe and triple U-tube. Applied Thermal Engineering, 2013, 61(2): 301-310.

[11] Cui P, Li X, Man Y, et al. Heat transfer analysis of pile geothermal heat exchangers with spiral coils. Applied Energy, 2011, 88(11): 4113-4119.

[12] Zhao Q, Liu F, Liu C, et al. Influence of spiral pitch on the thermal behaviors of energy piles with spiral-tube heat exchanger. Applied Thermal Engineering, 2017, 125: 1280-

1290.
[13] You T, Wu W, Shi WX, et al. An overview of the problems and solutions of soil thermal imbalance of ground-coupled heat pumps in cold regions. Applied Energy, 2016, 177: 515-536.
[14] Wu W, You T, Wang B, et al. Simulation of a combined heating, cooling and domestic hot water system based on ground source absorption heat pump. Applied Energy, 2014, 126: 113-122.
[15] You T, Wu W, Wang B, et al. Dynamic soil temperature of ground-coupled heat pump system in cold region. Proceedings of the 8th international symposium on heating, ventilation and air conditioning. Springer, Berlin, Heidelberg, 2014: 439-448.
[16] Cimmino M, Bernier M, Adams F. A contribution towards the determination of g-functions using the finite line source. Applied Thermal Engineering, 2013, 51(1-2): 401-412.
[17] Li Y, Mao JF, Geng SB, et al. Evaluating heat transfer models of ground heat exchangers with multi-boreholes based on dynamic loads, CIESC Journal, 2014, 65(3): 890-897. [in Chinese]
[18] Yu B, Wang FH, Yan L. Research on influence of space and arrangement between boreholes on the multi-pipe heat exchanger of GSHP. Refrigeration and air-conditioning, 2010, 10(5): 31-34.
[19] Rang HM, Study on zoning operation strategy of multi-borehole ground heat exchangers, Master dissertation, Jinan: Shandong Jianzhu University, 2017.
[20] Katsura T, Nagano K, Takeda S. Method of calculation of the ground temperature for

multiple ground heat exchangers. Applied Thermal Engineering, 2008, 28(14-15): 1995-2004.

[21] Go GH, Lee SR, Yoon S, et al. Design of spiral coil PHC energy pile considering effective borehole thermal resistance and groundwater advection effects. Applied Energy, 2014, 125: 165-178.

[22] Choi JC, Park J, Lee SR. Numerical evaluation of the effects of groundwater flow on borehole heat exchanger arrays. Renewable Energy, 2013, 52: 230-240.

[23] Loveridge F, Powrie W. G-Functions for multiple interacting pile heat exchangers. Energy, 2014, 64: 747-757.

[24] Gao J, Zhang X, Liu J, et al. Numerical and experimental assessment of thermal performance of vertical energy piles: an application. Applied Energy, 2008, 85(10): 901-910.

[25] Lee CK, Lam HN. A simplified model of energy pile for ground-source heat pump systems. Energy, 2013, 55: 838-845.

[26] Zhang W, Yang H, Lu L, et al. Study on spiral source models revealing groundwater transfusion effects on pile foundation ground heat exchangers, International Journal of Heat and Mass Transfer, 2015, 84: 119-129.

[27] Zhang W, Cui P, Liu J, et al. Study on heat transfer experiments and mathematical models of the energy pile of building. Energy and Buildings, 2017, 152: 643-652.

[28] Carslaw HS, Jeager JC, Conduction of heat in solids. 2th ed. Oxford Press, Oxford, 1959.

[29] Diao NR, Fang ZH, Ground-coupled heat pump technology, Higher Education Press, 2006.[in Chinese]

[30] Fang ZH, Diao NR, Cui P, Discontinuous operation of geothermal heat exchangers, Tsinghua Science and Technology, 2002, 7(2):194-197.

[31] Cui S, Zhang H, Zhang M. Swelling characteristics of compacted GMZ bentonite–sand mixtures as a buffer/backfill material in China. Engineering Geology, 2012, 141: 65-73.

[32] Assael MJ, Antoniadis KD, Metaxa IN, et al. A Novel Portable Absolute Transient Hot-Wire Instrument for the Measurement of the Thermal Conductivity of Solids. International Journal of Thermophysics, 2015, 36(10-11): 3083-3105.

[33] Li H, Liu Z, Xu Z, et al. Development of virtual simulation experiment for thermal conductivity and thermal diffusivity by using plane heat source method. Experimental Technology and Management, 2017, 34 (05): 5-7+10. [in Chinese].

[34] You T, Shi W, Wang B, et al. A new ground-coupled heat pump system integrated with a multi-mode air-source heat compensator to eliminate thermal imbalance in cold regions. Energy and Buildings, 2015, 107: 103-112.